Noname manuscript No.
(will be inserted by the editor)

Inertial effects on the vertical transport of suspended particles in a turbulent boundary layer

David Richter · Marcelo Chamecki

Received: DD Month YEAR / Accepted: DD Month YEAR

Abstract In many atmospheric flows, a dispersed phase is actively suspended by turbulence, whose competition with gravitational settling ultimately dictates its vertical distribution. Examples of dispersed phases include snow, sea spray droplets, dust, or sand, where individual elements of much larger density than the surrounding air are carried by turbulent motions after emission from the surface. In cases where the particle is assumed to deviate from local fluid motions only by its gravitational settling (i.e. they are inertialess), traditional flux balances predict a power law dependence of particle concentration with height. It is unclear, however, how particle inertia influences this relationship, and this question is the focus of this work. Direct numerical simulations are conducted of turbulent open channel flow, laden with Lagrangian particles of specified inertia; in this way the study focuses on the turbulent transport which occurs in the lowest few meters of the planetary boundary layer, in regions critical for connecting emission fluxes to the fluxes felt by the full-scale boundary layer. Simulations over a wide range of particle Stokes number, while holding the dimensionless settling velocity constant, are performed to understand the role of particle inertia on vertical dispersion. It is found that particles deviate from their inertialess behavior in ways that are not easily captured by traditional theory; concentrations are reduced with increasing Stokes number. Furthermore, a similarity-based eddy diffusivity for particle concentration fails as particles experience inertial acceleration, precluding a closed-form solution for particle concentration as in the case of inertialess particles. The primary

D. Richter
University of Notre Dame
Tel.: +574-631-4839
E-mail: David.Richter.26@nd.edu

M. Chamecki
University of California Los Angeles
Tel.: +310-825-0088
E-mail: chamecki@ucla.edu

consequence of this result is that typical flux parameterizations connecting surface emission models (e.g. saltation models or sea spray generation functions) to elevated boundary conditions may overestimate particle concentrations due to the reduced vertical transport caused by inertia in between; likewise particle emission may be underestimated if inferred from concentration measurements aloft.

Keywords atmospheric boundary layer · dispersion · dust · inertial particles · sea spray

1 Introduction

The planetary boundary layer (PBL) links the earth's surface to the atmosphere, and as a result controls the transmission of dust, salt, and other aerosols from their emission source at the surface to the larger meso- and synoptic-scale motions which govern their long-range transport and ultimate fate. Once airborne, these particulates can alter key chemical (O'Dowd and de Leeuw, 2007), optical (Kleefeld et al., 2002), and meteorological (Rosenfeld et al., 2008) processes before being deposited back onto the terrestrial or marine surface. Thus much work has been done in understanding and accurately parameterizing near-surface particle emission and transport processes for use in weather and climate prediction models, however continued discrepancies between models and observations remain a challenge (Knippertz and Todd, 2012; Reid et al., 2006). For instance the aircraft observation of large (up to $300\,\mu$m) sand grains above the Saharan Desert (Rosenberg et al., 2014) is in seeming contradiction with the upper limit of standard saltation models (Kok, 2011).

The difficulty of developing dust and aerosol emission schemes is due largely to unresolved, small-scale, and process-specific details, such as those resulting from wave breaking (Lewis and Schwartz, 2004) or saltation (Anderson and Haff, 1988). In this regard, the present work focuses on understanding the details of turbulent particle transport within the surface layer of the PBL — in particular the vertical flux of large particles which are heavy (i.e. they experience gravitational settling) and inertial (i.e. they do not necessarily follow fluid streamlines). It is the latter consideration, that of particle inertia, which is often neglected in particle flux parameterizations since even large sand grains or water droplets do indeed appear inertialess relative to PBL-scale motions. This work is focused, however, on turbulent transport which occurs in the lowest layers of the atmospheric surface layer (centimeters to meters above the surface), a region which plays the crucial role of connecting surface particle emission to transport throughout the full PBL, and where particle inertia can be non-negligible in their transport characteristics.

Attempts to parameterize heavy particle transport can begin by first approximating the suspended particulate as a passive scalar, in which case the horizontally-averaged vertical concentration profile and its relation to the surface flux could be described by Monin-Obukhov (MO) similarity theory (Monin and Yaglom, 1971). The particles can be made more realistic by adding a nonzero and constant settling velocity, which yields a power-law vertical profile under neutral conditions when assuming that the turbulent diffusivity of particle concentration is proportional to that of momentum (Prandtl, 1952; Rouse, 1937), and reflects an equilibrium balance between suspension via turbulence and gravitational settling. Other modifications, including disequilibrium between gravitational settling and turbulent suspension (Chamberlain, 1967; Kind, 1992), heterogeneous surface fluxes (Chamecki and Meneveau, 2011; Pan et al., 2013), non-neutral atmospheric stability (Freire et al., 2016), or various other meteorological effects specific to, for instance, sea salt aerorols (Toba, 1965) or snow (Pomeroy and Male, 1992), can be made as well.

It is well-known that particle inertia can lead to phenomena in turbulent flows such as preferential clustering (Rouson and Eaton, 2001) or turbophoretic drift (i.e. a net flux down a gradient of turbulent kinetic energy) (Reeks, 1983; Sardina et al., 2012), and these play a key role in determining inertial particle dispersion. For example, inhomogeneous horizontal particle distributions, such as those found in sand streamers (Baas, 2008), may disrupt the assumptions behind previous relationships. Much effort has gone into understanding inertial particle transport in turbulent channel flows, relating particle dynamics with turbulent events such as sweeps and ejections (Soldati and Marchioli, 2009; Righetti and Romano, 2004) or studying the modulation of turbulence via the suspended particles (Vreman, 2015), but many of these studies neglect the effects of wall-normal gravitational settling. In the presence of gravitational settling, particle clustering can lead to enhancements of the effective particle settling velocity (Wang and Maxey, 1993; Aliseda et al., 2002), where the average downwards particle velocity exceeds the still-air settling velocity as predicted by, say, Stokes drag.

In the PBL, while many theoretical and computational attempts have been made to characterize the Lagrangian dispersion characteristics of particles in turbulence (Wang and Stock, 1993; Csanady, 1963), it remains unclear how these effects of particle inertia modify the flux-profile relationship of particle mass concentration in the PBL, particularly in the lowest layers near the surface where Stokes numbers can be non-negligible. Even in theoretical studies devoted to the topic of vertical particle dispersion which attempt to include inertia, such as Belan et al. (2016), restrictions are necessarily made regarding the degree of particle inertia and the regions of the flow where the corrections are valid. Furthermore, in the well-known conceptual model for dry deposition (Slinn and Slinn, 1980; Slinn, 1982), the overall deposition velocity of particulate matter is represented as a series of resistances to vertical transport, including turbulence, molecular diffusion, and (when applicable) vegetative canopies. This conceptual model is the basis for many studies which aim to link surface emission to concentrations measured aloft — see for example Hoppel et al. (2002) or Fairall and Larsen (1984) — and within this framework particle inertia is only occasionally considered (Zhang et al., 2001; Peters and Eiden, 1992). When inertia is indeed included, it is only in the form of so-called inertial impaction, the process by which particles can efficiently travel through the diffusive sublayer due to inertia, thereby reducing the diffusive resistance to deposition.

The aim of the present study is to therefore investigate the role of particle inertia on modifying concentration profiles and vertical fluxes in the first several meters of the PBL. This is done using an idealized approach based on direct numerical simulation (DNS), and focuses on the flux-profile relationship and potential modeling strategies. It is ultimately demonstrated that particle inertia can reduce turbulent fluxes of particle concentration, which can create a disconnect between true surface emission fluxes and fluxes felt by the full PBL. In some sense this is akin to an additional inertial resistance layer in the conceptual model of Slinn and Slinn (1980), and could potentially cause miscalculations of surface fluxes or overprediction of suspended particulate matter.

2 Methodology

2.1 Numerical Simulation

2.1.1 Direct Numerical Simulation

The basis of this study is DNS of turbulent open channel flow, where Lagrangian particles are tracked individually. Details of the numerical method can be found in previous studies (Richter and Sullivan, 2013, 2014; Helgans and Richter, 2016), so only a brief summary will be included here. The neutrally-stratified, incompressible Navier-Stokes equations are solved in a Cartesian domain using a pseudospectral discretization in the homogeneous, periodic x and y directions and a second-order, finite difference discretization in the vertical, wall-normal z direction. Time integration is done via a low-storage, third order Runge-Kutta scheme (Spalart et al., 1991).

Mass and momentum conservation are given by:

$$\frac{\partial u_i}{\partial x_i} = 0, \tag{1}$$

$$\frac{\partial u_i}{\partial t} + u_j \frac{\partial u_i}{\partial x_j} = -\frac{1}{\rho_f}\frac{\partial p}{\partial x_i} + \nu_f \frac{\partial^2 u_i}{\partial x_j^2}, \tag{2}$$

where u_i is the fluid velocity, ρ_f is the fluid density, and ν_f is the fluid kinematic viscosity. Incompressibility is enforced by solving a pressure Poisson equation at each Runge-Kutta stage. A no-slip condition is imposed at the lower domain wall, and a no-stress condition is imposed at the upper wall. The horizontal directions are periodic, and the flow is driven by a constant pressure gradient, chosen to produce turbulent open channel flow with a Reynolds number of $Re_* = 300$, where $Re_* = u_* H/\nu_f$ is the friction Reynolds number based on the domain height H and the friction velocity $u_* = \sqrt{\tau_w/\rho_f}$ (τ_w is the wall stress).

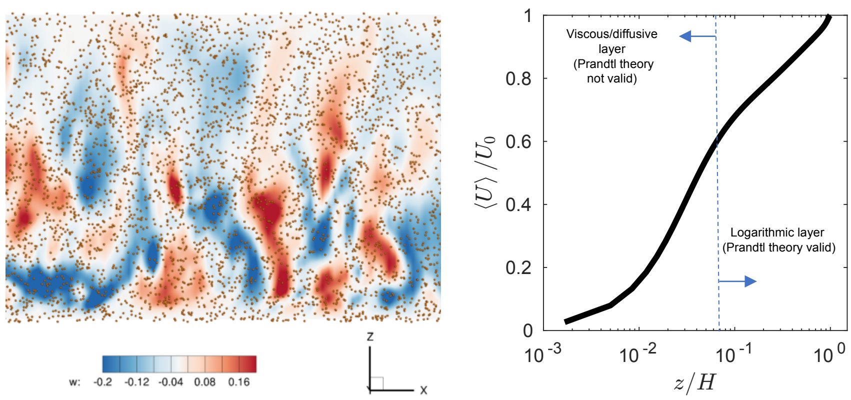

Fig. 1 Left: Snapshot of the computation. Colors reflect contours of fluctuating vertical velocity and brown dots represent Lagrangian particles. z axis in this figure has been magnified by a factor of 2.5. Right: mean velocity profile, showing the existence of a logarithmic layer above $z/H \approx 0.1$.

At the same time, an advection-diffusion equation for a passive scalar is computed as well:

$$\frac{\partial C}{\partial t} + \frac{\partial}{\partial x_j}(v_j C) = \mathit{\Gamma}_C \frac{\partial^2 C}{\partial x_j^2}, \tag{3}$$

where $\mathit{\Gamma}_C$ is the molecular diffusivity of scalar C. The concentration is advected by a velocity v_j, which is not necessarily equal to the local fluid velocity u_j. For instance, as done by Chamecki et al. (2009), this can be set to $v_j = u_j - w_s\delta_{j3}$ to represent uniform gravitational settling, where $w_s = \tau_p g$ is the single-particle particle terminal velocity specified by its inertial time constant τ_p and the gravitational acceleration magnitude g, and δ_{j3} is the Kronecker delta. A truly passive scalar would have $v_j = u_j$. In this study we assume a Schmidt number $Sc = \nu_f/\mathit{\Gamma}_C$ of unity. At the lower boundary, the Dirichlet condition $C \equiv C_0 = 1$ is held fixed, while at the upper boundary a no-flux condition is imposed. The domain is initialized with $C = 0$ at $t = 0$.

2.1.2 Lagrangian Particle Tracking

The primary goal of this study is to characterize the effects of particle inertia on turbulent fluxes and vertical concentration profiles in a turbulent boundary layer, and this is readily accomplished using Lagrangian methods (see e.g. Balachandar (2009)). Thus each simulation is seeded with a large number of Lagrangian point particles, whose ensemble-averaged concentration field is the scalar C governed by Eq. 3. The particles are assumed to be one-way coupled, in that they do not have any influence on the surrounding flow, since we assume here that the mass fraction of suspended particles is sufficiently low. In air suspended with solid or liquid particles, this approximation holds if the mass loading is roughly 1% or below (Balachandar and Eaton, 2010). Each particle obeys momentum conservation according to:

$$\frac{dv_{p,i}}{dt} = \frac{1}{\tau_p}\left(u_{f,i} - v_{p,i}\right) - g\delta_{i3}, \tag{4}$$

where $v_{p,i}$ is the particle velocity, g is the magnitude of gravitational acceleration, and $\tau_p = \rho_p d_p^2/18\rho_f \nu_f$ is the Stokes time scale. In these expressions d_p is the particle diameter, $u_{f,i}$ is the fluid velocity interpolated to the particle location, and ρ_p is the particle density.

In the limit of inertialess particles (i.e. the Stokes number $St \to 0$, where $St = \tau_p/\tau_f$ and τ_f is a relevant flow time scale; here we use the Kolmogorov time scale τ_K), Eq. 4 is not solved and rather the particle velocity is simply equal to the local fluid velocity less its terminal velocity:

$$v_{p,i} = u_{f,i} - \tau_p g \delta_{i3} = u_{f,i} - w_s \delta_{i3}. \tag{5}$$

In the further limit of massless particles, in which case the particles would simply represent a discretized form of a continuous passive tracer field, the particle velocity is equal to the local fluid velocity: $v_{p,i} = u_{f,i}$.

Given the restriction to relatively low Reynolds numbers due to the use of DNS, molecular diffusion of both momentum and scalar C occurs in a non-negligible region near the walls. To provide equivalency between the Lagrangian representation (i.e. the particles) and the Eulerian field C, the particles are moved according to a combination of their advection velocity $v_{p,i}$ and a Brownian step chosen to provide a diffusivity Γ_C:

$$dx_{p,i} = v_{p,i}dt + \sqrt{2\Gamma_C}d\xi_i, \tag{6}$$

where $d\xi_i$ is a Weiner process representing Brownian motion. Numerically, advection is solved using the same RK3 method used for the flow, and at the end of each time step, a random jump is added to provide the diffusive jump. Figure 1 provides a snapshot of the flow simulation with instantaneous particle location.

As noted above, the Eulerian scalar concentration C is held fixed at $C_0 = 1$ at the bottom wall, and a no-flux condition is imposed at the top wall. For Lagrangian particles, the same conditions are enforced: at the top wall, this means that particles are elastically reflected, and at the bottom wall, a reservoir of a constant number of particles just below the surface is maintained whose concentration is defined as $C_0 = 1$. The mean concentration $\langle C \rangle$ is then computed from a Lagrangian point of view at a specific height by counting the particles in the horizontal slab with volume $L_x \times L_y \times \Delta z$ (where L_x and L_y are the domain extents in the x and y directions and Δz is the vertical grid spacing at a particular height z) and normalizing with the concentration/volume combination maintained just below the bottom surface. This method requires a sufficient number of particles for statistical convergence of the particle averages, and in this case the number of particles maintained in the lower reservoir was held at 1×10^4 (this leads to particle numbers in the domain of $O(10^6)$).

Figure 2(a) shows a comparison between the Eulerian (Eq. 3) and Lagrangian prediction of $\langle C\rangle/C_0$ in the inertia-free case, for three different settling velocities. The settling velocities w_s are normalized by κu_* so that they reflect the settling tendency as compared to the strength of wall shear stress — in sediment transport literature this ratio is commonly referred to as the Rouse number (Rouse, 1937). Figure 2(a) demonstrates the equivalence between the Eulerian and Lagrangian particle treatment, including the adjustment of the advection velocity v_i in Eq. 3 by the settling velocity.

2.2 Existing theory

Following Prandtl (1952) (and many others since), the Reynolds decomposition $C = \langle C\rangle + c'$ can be introduced into Eq. 3, and after averaging the equations in absence of particle inertia and a net surface flux (e.g. Kind (1992)), one recovers a balance between turbulent suspension and gravitational settling:

$$\langle c'w'\rangle - \langle C\rangle w_s = 0 \tag{7}$$

If one then makes the assumption that the turbulent particle concentration flux $\langle c'w'\rangle$ can be expressed with an eddy diffusivity, in analogy with momentum and passive scalars, Eq. 7 becomes:

$$-K_C\frac{d\langle C\rangle}{dz} - \langle C\rangle w_s = 0, \tag{8}$$

where K_C is an eddy diffusivity. In the neutral atmospheric surface layer, Monin-Obukhov similarity theory implies $K_C = \kappa u_* z$ since the turbulent flux $\langle c'w'\rangle$ does not vary with height (here $\kappa = 0.41$ is the von Kármán constant and the turbulent Schmidt number is assumed to be unity). For open channel flow, however, the linearly varying momentum flux with height results in a parabolic diffusivity profile, given by $K_C = \kappa u_* z\,(1 - z/H)$ (see for example Fischer (1973)).

In its original formulation, the Prandtl solution to the ordinary differential equation of Eq. 8 suggests that the average concentration varies as a power law with height, with an exponent of $w_s/(\kappa u_*)$. Using the open channel version of K_C yields an equivalent result for systems where the total momentum flux varies linearly with height, which is a product of two power laws:

$$\frac{\langle C\rangle(z)}{C_r} = \left(\frac{z}{z_r}\right)^{-w_s/\kappa u_*}\left(\frac{z-H}{z_r-H}\right)^{w_s/\kappa u_*} \tag{9}$$

Here, z_r is a constant reference height where the mean concentration is C_r ($z_r = 0.3H$ in this work). Throughout the manuscript, the "Prandtl" solution will refer to Eq. 9, although it represents a profile in an open channel configuration where the eddy diffusivity K_C is parabolic with height, as opposed to the original atmospheric surface layer version (Prandtl, 1952). As noted previously, throughout the literature (particularly in relation to sediment transport) this profile is also sometimes referred to as the Rouse profile (Rouse, 1937).

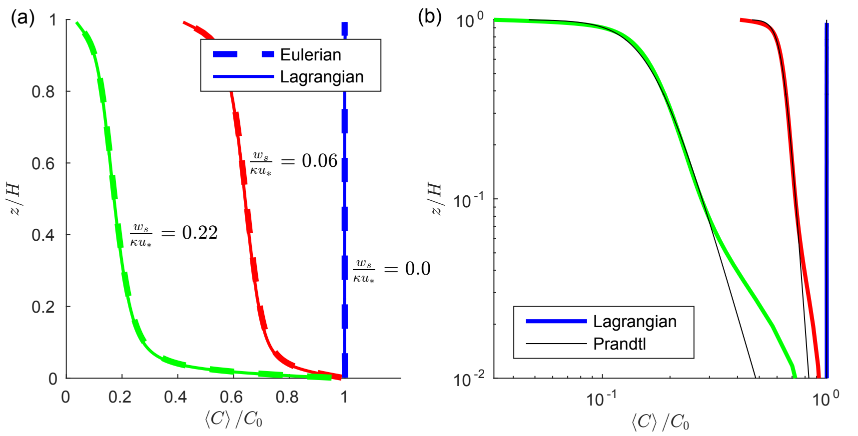

Fig. 2 Mean normalized particle concentration $\langle C \rangle / C_0$ versus normalized height z/H for three different settling velocities without inertia. Colors indicate different settling velocities and are indicated on the left. (a) Linear axes showing the comparison between the Eulerian solution (solid lines) and Lagrangian solution (dashed lines). (b) Logarithmic axes comparing the computed solutions to the Prandtl (1952) theory (Eq. 9).

Figure 2(b) shows that the Prandtl solution of Eq. 9 agrees very well with the concentration profiles computed in the inertialess cases, above a height of z/H around 0.1. Below this height, molecular diffusivity plays a large role (since the simulations are based on DNS), violating the basic assumption that the particle concentration is a result of a balance between turbulent suspension and gravitational settling. Thus in the absence of particle inertia, Eq. 9 accurately predicts concentrations over a range of settling velocities in regions of the flow where turbulence and gravity are indeed the dominant transport mechanisms.

3 Results and discussion

3.1 Interpretation

The numerical methodology outlined in the previous sections represents an idealized approach towards understanding the role of inertia in the flux-profile relationship of suspended particles. As such, we include here a brief discussion of both the applicability of the following results, as well as an explanation for how they should be interpreted.

First, the lower boundary conditions utilized for both the Eulerian and Lagrangian simulations are not intended to physically represent the process of particle emission from the surface. Since aeolian saltation at the sand/snow surface, droplet formation at the air-sea interface, lifting at the subaqueous sediment layer, etc. have widely varying physical explanations, the focus here is instead on the vertical transport of particles *once they have been suspended.*

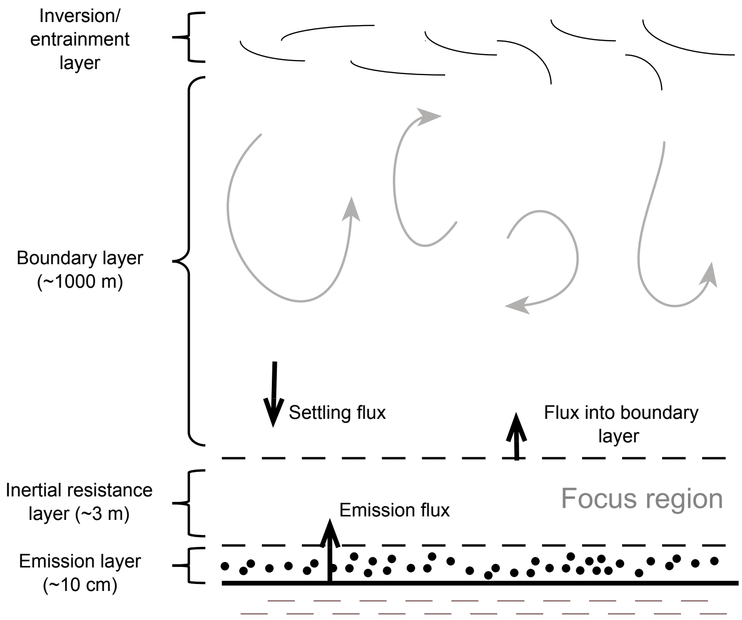

Fig. 3 Schematic detailing the structure of the PBL and the focus of the present DNS study. In the region above the emission layer and below the full boundary layer, local Stokes numbers can be large due to the rapid change in the turbulent kinetic energy dissipation rate with height, resulting in inertia-dominated transport of particles in the bottom few meters of the PBL. The emission layer includes the region where processes such as bubble bursting or saltation occur, which are not explicitly represented in this study.

In the present work, molecular diffusion, as represented by Brownian motion for the Lagrangian particles and by a constant molecular diffusivity for the Eulerian concentration field, is used as a means for achieving this suspension, in the sense that it is responsible for carrying particles from the specified concentration at the surface to a level where turbulence dominates transport (this occurs at a level of $z/H \approx 0.1$ in the DNS presented here). This allows for a direct comparison between the Eulerian and Lagrangian methods, and allows us to focus instead on the turbulent transport in regions above this layer. How the particles have arrived this this height is immaterial for our purposes.

Second, the DNS framework is meant to represent only the lowest few meters of the PBL where inertia is present (the "inertial resistance layer" — see Fig. 3). Thus the parameter H in the simulations is not the boundary layer height of $O(1000\,\mathrm{m})$ but rather the top of the inertial resistance layer which has a height of $O(1\,\mathrm{m})$. For a given particle size, the Stokes number computed based on the local Kolmogorov time scale changes very rapidly with height, leaving a region near the surface (but above the emission layer) where inertia can be large. The depth of this layer is controlled by both the particle size and the turbulence levels in the boundary layer. Since $St = \tau_p/\tau_K$ depends on both τ_p and the local Kolmogorov time scale, the depth of this layer would scale as d_p^2, since τ_p is proportional to d_p^2, and with $u_*^{3/2}$, since the turbulent kinetic energy dissipation rate ϵ is proportional to u_*^3 and τ_K is proportional to $\epsilon^{-1/2}$ (at least in neutral conditions). As demonstrated below in section 3.6, the features observed in the DNS can be felt throughout larger-scale models which cannot resolve these small-scale motions and instead resolve PBL-scale motions.

3.2 Adding particle inertia

The goal of this work is to extend the analysis of section 2.2 to include particles which exhibit appreciable inertia during their turbulent transport. In most studies on this topic (Chamberlain, 1967; Chamecki et al., 2009; Kind, 1992), particle inertia is neglected and only gravitational settling is taken into consideration. In other studies (Belan et al., 2016; Csanady, 1963; Freire et al., 2016), particle inertia is treated insofar as it is responsible for altering dispersion rates, and compared to the large scales associated with the full PBL the effect of inertia is quite small. Here, our focus is on the lowest layers of the particle-laden boundary layer, where the transport is crucial for linking the small-scale emission processes with the large-scale PBL.

With this in mind, we design a set of numerical experiments whose purpose is to systematically vary the particle inertia while holding the settling tendency the same, in order to determine the effects on the average concentration profiles and flux characteristics. A nondimensional settling velocity of $w_s/(\kappa u_*) = 0.06$ is held fixed (red lines in Fig. 2), and the flow Reynolds number is likewise fixed at $Re_* = 300$. The particle inertial time scale τ_p is then varied to provide Stokes numbers ranging between $St = 0.05$ and $St = 5.0$. We note that the following analysis only reports results from a single nondimensional settling velocity, but the same general results are found at other values of $w_s/(\kappa u_*)$. The effect of w_s is to modify the baseline concentration profile, from which inertia modifies as described below. We also note that while holding w_s constant while varying St is artificial, it allows us to target explicitly the effects of inertia, without confounding them with changes in w_s at the same time. In reality, w_s and St are linked via τ_p, although local values of St can change with height.

For our DNS, we use a flow time scale of $\tau_f = \overline{\tau}_K$ to define St, where $\overline{\tau}_K$ is the vertically-averaged Kolmogorov time scale in the channel. For reference, if one uses the logarithmic scaling of viscous dissipation rate in the atmospheric surface layer, $\epsilon = u_*^3/\kappa z$, then $\overline{\tau}_K$ averaged over the lower 5 meters of the surface layer for $u_* = 0.4\,\mathrm{m\ s^{-1}}$ is roughly 0.015 seconds. In these conditions the Stokes number range of $St = 0.5$ to $St = 5.0$ corresponds to diameters of $d_p \approx 10\,\mu\mathrm{m}$ to $d_p \approx 150\,\mu\mathrm{m}$ when the particle density is of order $1000\,\mathrm{kg\ m^{-3}}$. Thus spray droplets or dust particles suspended in air can quite easily behave

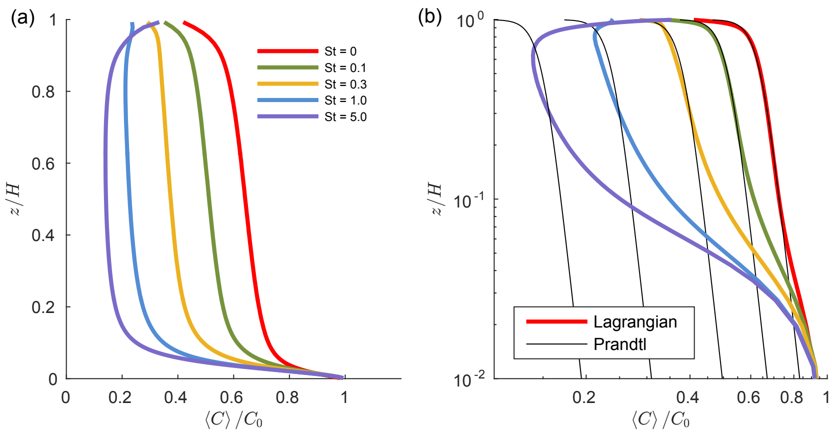

Fig. 4 (a) Average normalized concentration $\langle C\rangle /C_0$ computed from the inertial, Lagrangian simulations as a function of z/H. The settling velocity is held fixed at $w_s/(\kappa u_*) = 0.06$ for all cases, and $Re_* = 300$. (b) The same concentration profiles on logarithmic axes, with Eq. 9 plotted in thin black lines for reference. The addition of inertia dramatically changes the concentration within the domain, and causes the average profile to deviate significantly from the inertialess theory.

as inertial particles within $O(1\,\mathrm{m})$ of the surface (i.e. the "inertial resistance layer" found in Fig. 3).

Figure 4(a) presents the normalized average concentration profiles as a function of z/H over the range of St considered. Despite the settling velocity being identical between these cases, the addition of inertia clearly inhibits the ability of particles to distribute vertically throughout the domain. Over the present range of St, this trend is monotonic, in that higher St leads to lower mean concentrations throughout the entire channel. The exception is the $St = 5.0$ case, where upwards turbophoretic drift (Reeks, 1983; Sardina et al., 2012) actually overcomes gravitational settling, pushing particles towards the top wall and increasing concentrations there (i.e. the finite size of the domain begins to contaminate the solution since vertical velocity fluctuations must approach zero at the top wall).

Figure 4(b) illustrates that the Prandtl theory describing the vertical profiles of concentration as a balance between turbulent flux and gravitational settling fails significantly as St is increased (thin black lines). At low St, Eq. 9 is still accurate in the upper regions of the domain, but the height range over which agreement is found diminishes. The disagreement propagates from the bottom, since the local Stokes number, as computed by the local value of τ_K, is a monotonically decreasing function with height. Thus the first regions of the flow where the theory begins to fail are those where the local St is locally large enough to cause the particles to cease acting like settling, passive tracers.

By solving Eq. 3 and only considering gravitational advection (i.e. $v_j = u_j - w_s\delta_{j3}$), the turbulent flux $\langle c'w'\rangle$, diffusive flux $-\Gamma_C\left(\partial \langle C\rangle /\partial z\right)$, and gravitational flux $-w_s\langle C\rangle$ are computed directly from the Eulerian concentration field. Simultaneously, the same flux quantities can be computed from the Lagrangian particles as well. The gravitational flux is still $-w_s \langle C \rangle$ (using the Lagrangian-based $\langle C \rangle$), and Reynolds averaging of the particle evolution equations shows that the sum of the turbulent and gravitational fluxes is equal to $\langle w_p \rangle \langle C \rangle$, where $\langle w_p \rangle$ is the average particle vertical velocity. Therefore the turbulent flux (counterpart to $\langle c'w' \rangle$ in the Eulerian frame) is the difference between the gravitational flux and the concentration-weighted average particle velocity. Finally, the total flux is computed from the Lagrangian point of view by keeping track of the net number of particles crossing each horizontal plane in each time step. From this total, the gravitational and turbulent fluxes can be subtracted to yield the diffusive flux.

First, to demonstrate that the Eulerian versus Lagrangian-based flux calculations are equivalent for systems with no inertia, Fig. 5 shows the Lagrangian-computed profiles in thick red lines and the Eulerian-computed fluxes thin black lines for the inertialess case shown in Figure 4. It is clear that the flux profiles in this case are nearly identical, and therefore the Lagrangian-based fluxes are accurate representations of vertical particle transport.

Several features are of note in Fig. 5. First, since we average only after the system has reached steady state, the total flux should be zero, which Fig. 5 indeed indicates is the case. Figure 5 shows that in this steady state condition, above $z/H \approx 0.1$ and below $z/H \approx 0.9$, the flux balance, even in the presence of substantial particle inertia, is strictly between gravitational settling and turbulent suspension. As expected, this spatial region corresponds to the region of Fig. 4 where the Prandtl-predicted concentration profile agrees with the simulations in the absence of particle inertia. Near the top and bottom walls, turbulent fluxes are replaced by nonzero diffusive fluxes, thus violating the assumptions behind the Prandtl theory.

Figure 5 also illustrates that within the regions unaffected by diffusion, increases in particle inertia suppress turbulent fluxes, which are in turn balanced by lower gravitational settling fluxes. So while the dominant balance remains between turbulence and gravity, their magnitudes have deviated sharply from the noninertial case. This trend increases with St, and the inertialess Eulerian formulation (thin black lines) is clearly insufficient in predicting the fluxes for inertial particles.

3.3 Inertial correction to the advection velocity

In order to capture inertial effects in the Eulerian calculations, we utilize an inertial correction to the advection velocity v_j in Eq. 3 which is based on an asymptotic expansion of equation 4 in Stokes number, retaining only the first order correction (Druzhinin, 1995; Maxey, 1987). More recent implementations of this correction have acquired the name of the "Equilibrium Eulerian" model, whose advantage is that it captures some inertial affects while still allowing the particle advection velocity to be written in terms of local flow velocities and accelerations (Ferry and Balachandar, 2001; Balachandar, 2009).

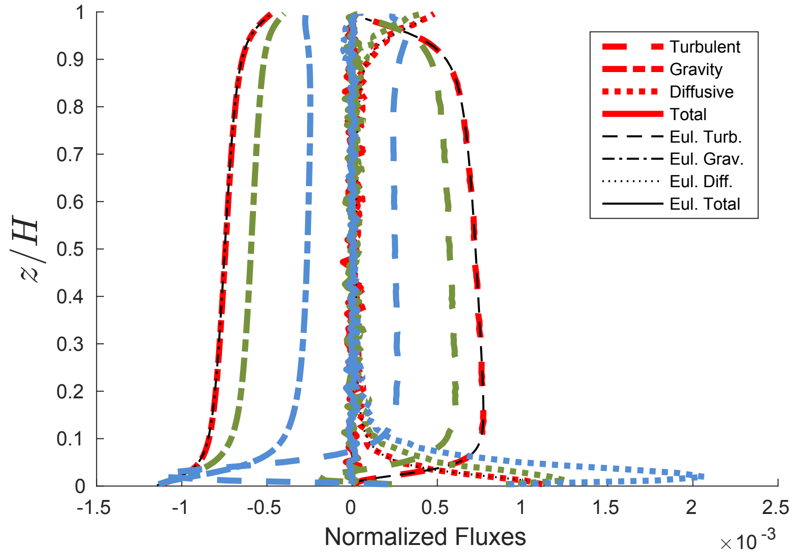

Fig. 5 Vertical profiles of concentration fluxes for a subset of the overall Stokes numbers: $St = 0$ (red), $St = 0.1$ (green), and $St = 1.0$ (blue). Line types provided in the legend refer to the turbulent flux, the gravitational flux, the diffusive flux, and the total flux. The thick colored lines refer to fluxes computed from the Lagrangian particle data; thin black lines are fluxes from an Eulerian, inertialess perspective. Fluxes normalized by C_0U_0, where U_0 is the maximum velocity in the channel.

Under this approximation, the advection velocity takes the form:

$$v_j = u_j - w_s\delta_{j3} - \tau_p \frac{Du_j}{Dt}, \tag{10}$$

where $\frac{D}{Dt} = \frac{\partial}{\partial t} + u_k \frac{\partial}{\partial x_k}$ is the total fluid acceleration. The meaning of the last term in Eq. 10 is that the fluid velocity seen by the particle at a time τ_p before the present time should be factored into the current particle velocity due to inertia, and would only be expected to be accurate below $St \approx 0.2$ since the correction is only first order (Ferry and Balachandar, 2001).

Following the same Reynolds averaging procedure as done for deriving Eq. 7, this correction to the advection velocity leads to two additional terms in the vertical flux balance:

$$\langle c'w' \rangle - \langle C \rangle w_s - \langle C \rangle \tau_p \frac{\partial \langle w'^2 \rangle}{\partial z} - \tau_p \left\langle c' \frac{Dw'}{Dt} \right\rangle = 0. \tag{11}$$

The first two terms are the same turbulent and gravitational settling fluxes from Eq. 7. The third term on the left hand side of Eq. 11 represents turbophoresis, where inertia causes a drift against gradients of turbulent kinetic energy (Reeks, 1983), and the fourth term on the left hand side represents correlations between concentration fluctuations and vertical accelerations. It

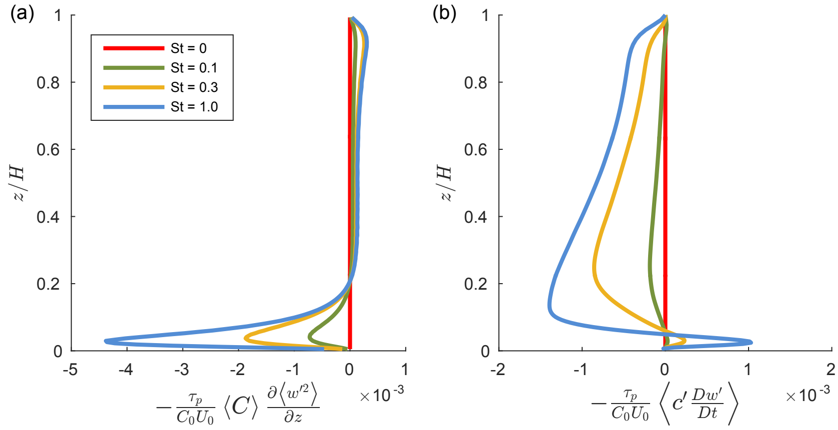

Fig. 6 Additional, inertia-based flux terms in Eq. 11 as a function of height. Different lines refer to different Stokes numbers ranging between 0 and 1.0 (see legend). (a) turbophoresis term: $-\tau_p \langle C \rangle \frac{\partial \langle w'^2 \rangle}{\partial z}$, (b) correlation between concentration fluctuations and vertical accelerations: $-\tau_p \left\langle c' \frac{Dw'}{Dt} \right\rangle$. Both terms normalized by $C_0 U_0$.

can be easily shown that the sum of these two terms is simply $-\tau_p \left\langle C \frac{Dw'}{Dt} \right\rangle$, i.e., the correlation of the total concentration with vertical acceleration.

With this formulation in mind, we perform a new simulation in which v_j in Eq. 3 is replaced by Eq. 10 in order to compare its predictions with the true behavior of the inertial Lagrangian particles (here "true" indicates that we expect the theory to match the Lagrangian simulations exactly if the theory were correct). From these calculations, Fig. 6 presents the two extra flux terms in Eq. 11 as a function of height for a range of St, which shows that each of the inertial corrections to the vertical flux are of the same order of magnitude. As expected, the turbophoretic term in Fig. 6(a) is largest in the regions near the lower wall where the gradients of the turbulent kinetic are the highest. These profiles are related to one another, in the sense that the gradient $\frac{\partial \langle w'^2 \rangle}{\partial z}$ is the same in all cases since the underlying turbulence has not changed with particle Stokes number.

In the range where molecular diffusion is unimportant (above $z/H \approx 0.1$), the concentration fluctuation/vertical acceleration correlation term (Fig. 6(b)) is dominant and negative, suggesting that inertia tends to reduce the vertical flux. This is in agreement with the Lagrangian-based fluxes computed in Fig. 5, and provides an Eulerian interpretation of this suppression of the concentration flux. It is noteworthy that the dominance of this term over the turbophoretic term indicates that inertial corrections to vertical dispersion must include additional effects beyond turbophoretic drift. As the particle Stokes number increases, these flux corrections generally become larger since they are proportional to τ_p, although the correlation saturates around $St = 0.5$. We note that the corrections for $St = 5.0$ are not shown since the inertia-corrected ad-

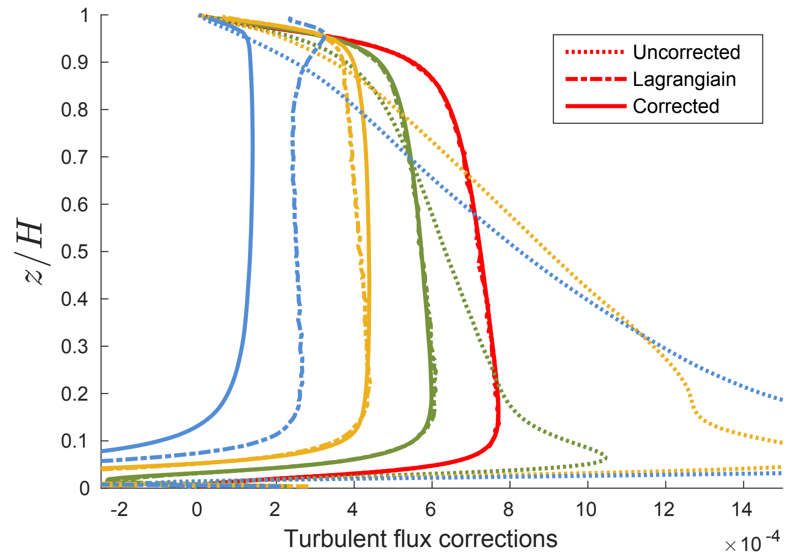

Fig. 7 Turbulent fluxes with inertial correction to Eulerian advection velocity. Uncorrected turbulent flux $\langle c'w' \rangle$ (dashed), Lagrangian turbulent flux (dash-dotted), and the corrected turbulent flux $\langle c'w' \rangle_{corr}$ (solid). Line colors refer to legend in Fig. 6. Axes have been zoomed in to better highlight agreement between the Lagrangian-based fluxes and the corrected Eulerian fluxes.

vection velocity causes the numerical simulations to become unstable at such high values of τ_p.

If one interprets the last two terms of Eq. 11 as a correction to the inertialess turbulent flux, then a corrected turbulent flux can be defined:

$$\langle c'w' \rangle_{corr} = \langle c'w' \rangle - \langle C \rangle \tau_p \frac{\partial \langle w'^2 \rangle}{\partial z} - \tau_p \left\langle c' \frac{Dw'}{Dt} \right\rangle \tag{12}$$

which should approach the Lagrangian-computed turbulent flux for the inertial particles presented in Fig. 5. Figure 7 shows that this is indeed the case, however beginning at $St \approx 0.3$ the linear correction begins to break down. In this figure, the turbulent flux $\langle c'w' \rangle$ ("uncorrected" in Fig. 7) far overpredicts the vertical turbulent flux over much of the domain when v_j is modified to include the inertia. When adding the additional flux terms of Eq. 11 to $\langle c'w' \rangle$ ("corrected" in Fig 7), the vertical turbulent flux nearly exactly matches the true flux predicted from the Lagrangian particles. While the corrected Eulerian flux diverges from the Lagrangian beginning at $St \approx 0.3$, the flux is fairly accurate through $St = 0.5$, suggesting that the key inertial effects on vertical fluxes have been captured by the linear correction to v_j. The resulting predictions of the vertical concentration profiles are likewise accurate up to $St \approx 0.3$, as shown in Fig. 8. The degree of success of inertial correction to v_j

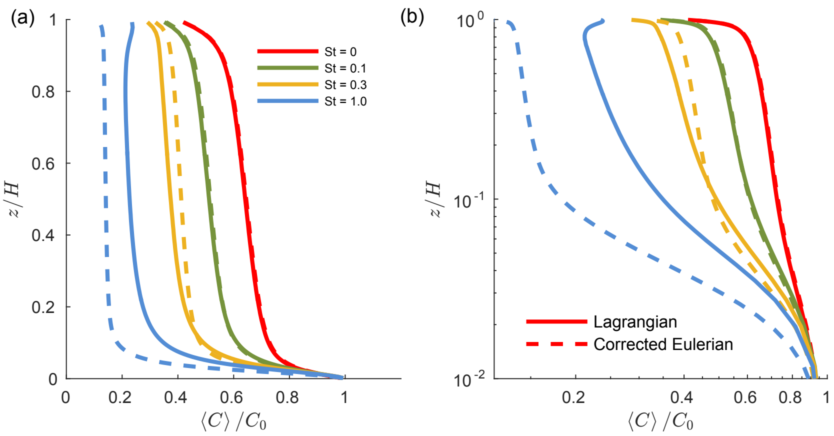

Fig. 8 Concentration profiles as predicted by the Lagrangian particles (solid lines) and the corrected Eulerian field (dashed lines). (a) Linear axes, (b) Logarithmic axes.

is in complete agreement with previous uses of the Equlibrium Eulerian model (Ferry and Balachandar, 2001).

3.4 Revisiting the Prandtl theory

The Prandtl solution for concentration (Eq. 9) was derived assuming a balance between turbulent suspension and gravitational settling. Furthermore, it uses a parabolic form of the eddy diffusivity, i.e., $K_C = \kappa u_* z\,(1 - z/H)$, which is the eddy diffusivity predicted by MO similarity theory in the presence of a linear momentum flux. As a first step, therefore, we compute K_C in the case of inertial particles to see how well a parabolic function compares with the eddy diffusivity implied by the ratio of the turbulent flux to the mean concentration gradient. For the corrected Eulerian flux this follows:

$$K_{C,E} = -\frac{\langle c'w' \rangle_{corr}}{\frac{\partial \langle C \rangle}{\partial z}}, \tag{13}$$

while for the Lagrangian-computed turbulent flux K_C is computed as:

$$K_{C,L} = -\frac{\left(\langle w_p \rangle + w_s\right)\langle C \rangle}{\frac{\partial \langle C \rangle}{\partial z}}, \tag{14}$$

where the numerator is the turbulent flux measured from the Lagrangian particles, and inherently includes all true inertial effects.

Figure 9 shows both $K_{C,E}$ and $K_{C,L}$, and compares them to the parabolic solution assumed by MO theory. It is clear that the inertialess case ($St = 0$, red lines) follows the parabolic solution fairly closely, which is expected since the Prandtl solution was successful at predicting the mean concentration profiles

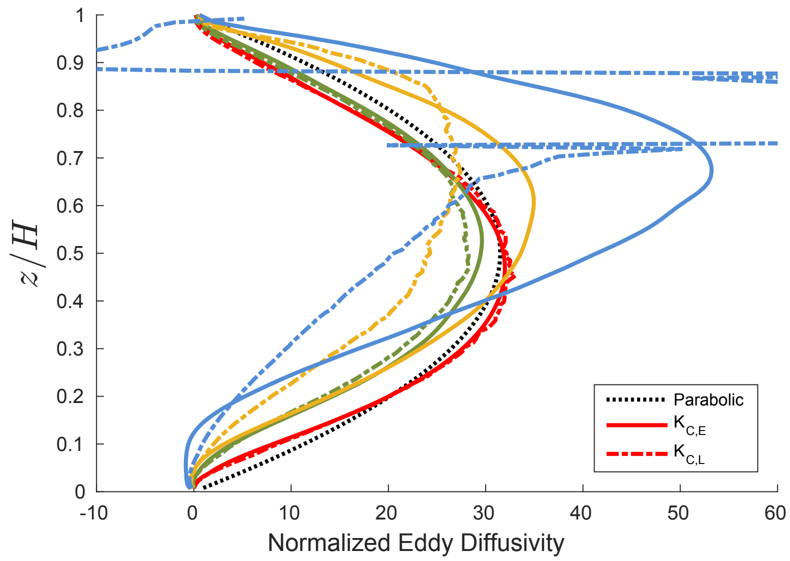

Fig. 9 Eddy diffusivities normalized by the molecular diffusivity Γ_C. Dotted black line represents the parabolic solution $K_C = \kappa u_* z(1 - z/H)$. Solid lines represent $K_{C,E}$ and dash-dotted lines represent $K_{C,L}$. Both profiles have been smoothed with an averaging filter. Colors follow legend of Fig. 8.

in Fig. 4. As St increases, however, not only do the computed eddy diffusivities deviate from the parabolic approximation, the Eulerian and Lagrangian predictions deviate from one another. Again, this is expected given the deviation between the corrected Eulerian and Lagrangian profiles shown in Fig. 7 and Fig. 8, since the Eulerian correction is only valid at low St. We note that the difference between $K_{C,L}$ and the parabolic solution is not simply a result of the so-called crossing trajectories effect: the correction proposed by Csanady (1963) for the vertical eddy diffusivity results in a vertical dispersion coefficient that is less than 1% different than the parabolic solution.

While the shape of both $K_{C,E}$ and $K_{C,L}$ is still somewhat parabolic at $St = 0.3$ (yellow lines in Fig. 9), the emergence of an inflection point in the concentration profile at $St = 1.0$ (see Fig. 8) causes $K_{C,L}$ to spike to very large and even negative numbers near $z/H \approx 0.8$. This behavior indicates that inertial particles violate the basic flux-gradient relationship assumed when defining an eddy diffusivity K_C, although the inertial correction to the Eulerian advection velocity compensates for this up to $St \approx 0.2$, as noted earlier.

It is instructive therefore to repeat the Prandtl analysis and attempt to predict the concentration profile while incorporating the inertial corrections to the Eulerian concentration field. The goal here is to determine whether or not a parabolic eddy diffusivity can be utilized for the uncorrected turbulent flux $\langle c'w' \rangle$ while capturing the inertial effects separately and explicitly. If this fails (which it indeed does), it would indicate that inertial effects must be accounted for in the eddy diffusivity itself and not as a series of correction terms to the overall flux balance. If Eq. 11 is written as:

$$\langle c'w' \rangle - \langle C \rangle w_s + \beta(z) = 0, \tag{15}$$

where $\beta(z)$ represents the inertial corrections to the turbulent flux,

$$\beta(z) = -\langle C \rangle \tau_p \frac{\partial \langle w'^2 \rangle}{\partial z} - \tau_p \left\langle c' \frac{Dw'}{Dt} \right\rangle, \tag{16}$$

the analog to Eq. 8 assuming the parabolic form of the eddy diffusivity K_C is:

$$\kappa u_* z (1 - z/H) \frac{d \langle C \rangle}{dz} + \langle C \rangle w_s = \beta(z). \tag{17}$$

The solution to this inhomogeneous equation takes the following form:

$$\begin{aligned} \frac{\langle C \rangle (z)}{C_r} &= \left(\frac{z}{z_r} \right)^{-w_s/\kappa u_*} \left(\frac{z - H}{z_r - H} \right)^{w_s/\kappa u_*} \\ &+ \left(\frac{z}{H - z} \right)^{-w_s/\kappa u_*} \int_{z_r}^{z} \left(\frac{z}{H - z} \right)^{w_s/\kappa u_*} \frac{\beta(z)}{C_r \kappa u_* z (1 - z/H)} dz. \end{aligned} \tag{18}$$

Equation 18 contains the original Prandtl solution of Eq. 9 as the first term, followed by a correction which involves an integral of the inertial correction term $\beta(z)$. Since we do not have a closure for this term, we must integrate this term numerically, and its solution is presented in Fig. 10. Note that since $\langle C \rangle$ appears in the definition of $\beta(z)$, the numerical solution must be iterative; since the term containing $\langle C \rangle$ is small above $z_r = 0.3$ (Fig. 6(a)), however, the solution converges very rapidly.

Figure 10 shows that the correction indicated by Eq. 18 does not adequately modify the original Prandtl solution to account for inertia. This is of course true at the highest values of St (since again the inertial correction only is valid at low St), but even at $St = 0.3$ the additional term in Eq. 18 overcorrects the Prandtl solution substantially.

The reason behind this discrepancy is that the similarity-based, parabolic form of the eddy diffusivity K_C is no longer valid as St increases. If Eq. 8 is written using the Lagrangian-based $K_{C,L}$ as:

$$-K_{C,L} \frac{d \langle C \rangle}{dz} - \langle C \rangle w_s = 0, \tag{19}$$

then the solution for $\langle C \rangle$ can be computed numerically using the $K_{C,L}$ profiles presented in Fig. 9 (i.e. the dash-dotted lines). Note that Eq. 19 does not contain the inertial correction term $\beta(z)$ since the Lagrangian-based $K_{C,L}$ inherently includes all inertial effects. Figure 10 shows that when solving Eq. 19, the predicted concentration profile very closely matches the Lagrangian-based concentration profiles, except for regions near the inflection points in $\langle C \rangle$ where $K_{C,L}$ is ill-defined. Thus, the effects of particle inertia on vertical dispersion must not be limited to corrections to the turbulent flux (e.g. using

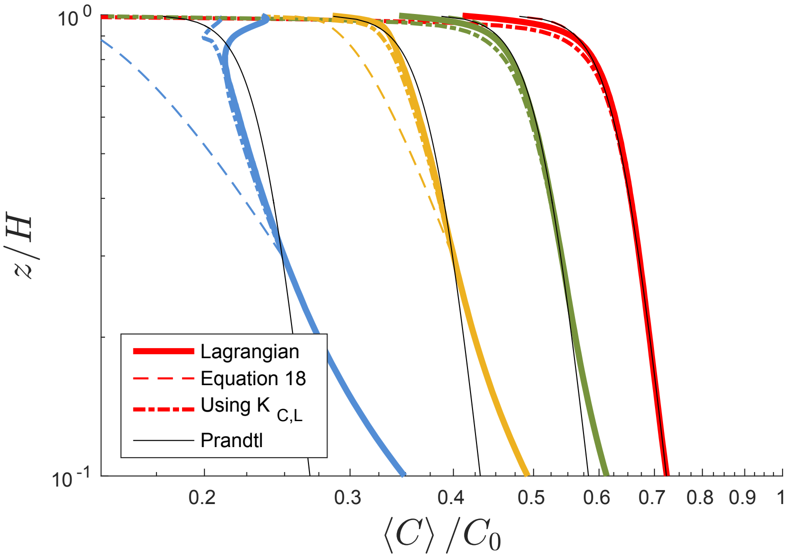

Fig. 10 Vertical concentration profiles computed from the inertial Lagrangian particles (solid lines) compared to the prediction of Eq. 18 (dashed lines). As before, $z_r = 0.3H$ and C_r is the concentration at this height, so the solution to Eq. 18 only exists above $z/H = 0.3$. Dash-dotted lines are the numerical solutions to Eq. 19, which uses the Lagrangian-based $K_{C,L}$, illustrating that the parabolic K_C becomes insufficient at high St. Colors refer to the legend in Fig. 8.

the Equilibrium Eulerian model to correct the particle advection velocity), but must also consider the fact that the eddy diffusivity, and therefore the relationship between the flux and the mean concentration gradient, is modified by inertia as well.

3.5 Reynolds number

Before demonstrating the effect of the inertial resistance layer in larger-scale models, we provide a comment upon the usage of direct numerical simulation, and thus the limitation in Reynolds number, of the current work. As the Reynolds number of this type of simulation increases towards the types of atmospheric flows we aim to investigate, the primary effect is to reduce the region over which molecular momentum and scalar diffusion dominate; indeed it is only outside of this region that the present work has focused. To this end, two additional simulations were run at a Reynolds number of $Re_\tau = 700$ in order to demonstrate that the primary conclusions of this work remain intact. Figure 11 shows the counterparts to Figs. 4(b) and 9 for an inertialess and a $St = 0.1$ particle at the same dimensionless settling velocity. Figure 11(a) shows that again, the inclusion of particle inertia causes a reduction in the concentration profile, and that the deviation from the Prandtl solution

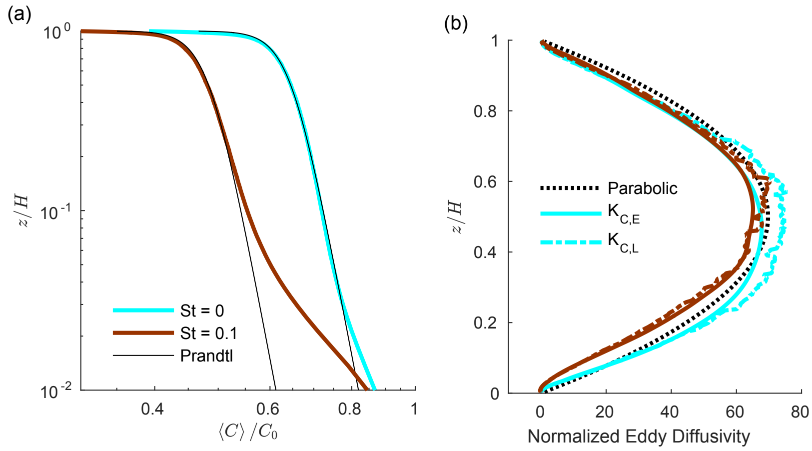

Fig. 11 (a) Concentration profiles and (b) eddy diffusivity profiles for $Re_\tau = 700$ cases for $St = 0$ (cyan) and $St = 0.1$ (dark red) particles. The trends are nearly identical to those presented in Figs. 4(b) and 9, respectively, illustrating the robustness of the present conclusions with increasing Re.

propagates from the lower wall upwards, beginning in regions with high local St. The only difference with the increased Reynolds number is that the range of agreement of the $St = 0$ case with the Prandtl solution extends further towards the lower surface, to $z/H \approx 0.02$ as opposed to $z/H \approx 0.08$ as before. The same is true in Fig. 11(b): the presence of inertia begins to alter the eddy diffusivity profile in a similar way to that of the lower Re cases, only in this case the magnitude of K_C is larger (as expected). Thus we argue that the methodology of using DNS as a tool for studying inertial particle fluxes in the lowest regions of the atmospheric surface layer is justified in that the effects of Reynolds number do not appreciably alter our basic findings.

3.6 Consequence of the inertial resistance layer

We argue above that within the first few meters above the emission layer, particles often experience inertial effects as they are carried upwards by turbulent motions. In the DNS this is manifested as a reduction of the concentration profile at steady state, but can also be described as a reduction in the vertical turbulent flux above a particle source, similar to classic descriptions of deposition velocity resistance via molecular diffusion or vegetation canopies (Slinn and Slinn, 1980). In practice, this reduction in turbulent flux near the surface effectively reduces the emission flux felt by the boundary layer as compared to the true source flux. In this study we use DNS to resolve these near-wall motions to study their effect, but in practice these motions cannot be resolved and thus their effect must be parameterized.

To demonstrate this process, we perform a representative large eddy simulation (LES) using the unstable convective PBL studied in Freire et al. (2016).

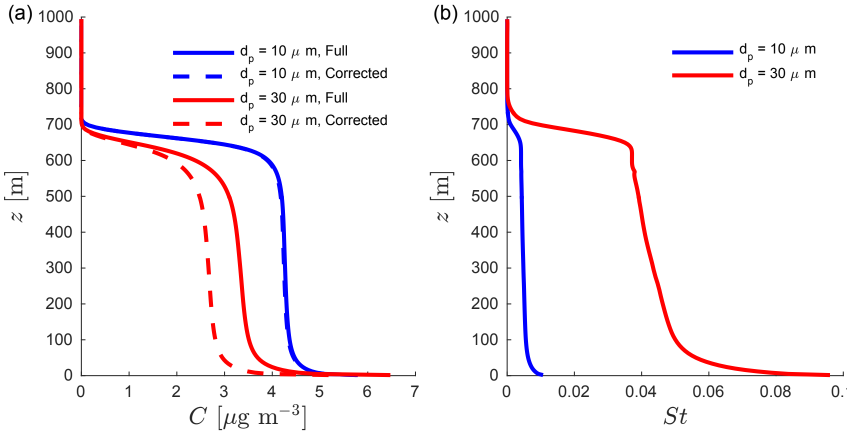

Fig. 12 (a) Concentration profiles of $d_p = 10\,\mu$m (blue) and $d_p = 30\,\mu$m (red) particles for the unstable convective PBL of Freire et al. (2016). Solid curves represent full surface fluxes of $0.2\,\mu$g m^{-2}!s^{-1} and dashed lines represent surface fluxes corrected for inertial transport between the first grid point and the emission layer. (b) Stokes numbers of $d_p = 10\,\mu$m and $d_p = 30\,\mu$m particles, as computed by the subgrid dissipation of the LES scheme. From the perspective of LES, these particles are nearly inertialess, but can have significant inertial effects near the surface.

For an initial boundary layer height of $z_i = 570\,$m, a surface heat flux of 0.24 K m s^{-1}, and a geostrophic wind of $U_g = 10\,$m s^{-1}, Eulerian concentration fields of $d_p = 10\,\mu$m and $d_p = 30\,\mu$m particles are solved, only taking into account gravitational settling and not explicitly accounting for inertia.

In Fig. 12(a), the solid curves represent the concentration profiles averaged between hours 3 and 4 for the same surface emission flux of $0.2\,\mu$g m^{-2} s^{-1}. As expected, the heavier particles have lower concentrations throughout the PBL. To account for inertial effects at and beneath the first LES grid point, we estimate a surface Stokes number based on LES dissipation at the first grid point, and use Fig. 7 to provide a corresponding reduction in the surface flux due to the inertial resistance layer. For the case of $d_p = 10\,\mu$m particles, the local Stokes number at the bottom grid point is $St \approx 0.01$ and the corrected flux is estimated to be 99% of the original surface flux; the dashed blue line in Fig. 12(a) reflects this small difference. For the case of $d_p = 30\,\mu$m (dashed red line), however, the surface Stokes number is $St \approx 0.1$ and the reduction in surface flux is roughly 22%. Figure 12(a) highlights the fact that, as a result of this near-surface reduction of turbulent flux, mean concentrations throughout the entire PBL can be influenced by inertia near the surface. Furthermore, Fig. 12(b) shows that while inertial effects can lead to substantial changes in the predicted large-scale concentrations, particles in these regions do indeed appear nearly inertialess at these scales, as computed by their local Stokes number. Only near the surface do they begin to experience inertial effects, even possibly throughout the surface layer (see for example Nemes et al. (2017)). We again emphasize that the region of interest in this study, as simulated by

DNS, is within several meters of the surface (Fig. 3). By definition, LES in general cannot resolve the observed inertial behavior of the particles because it is a processes which occurs at the smallest scales of the turbulent flow.

4 Conclusions

In this work we seek to better understand the influence of particle inertia on vertical concentration profiles, and in particular the shortcomings of traditional relationships that work well in low- or zero-inertia conditions (e.g. Prandtl (1952)). We utilize direct numerical simulations and Lagrangian point particles in turbulent open channel flow to explore the ability of inertial corrections to the Eulerian transport equation (i.e. the Equilibrium Eulerian model (Ferry and Balachandar, 2001)) to capture changes in the turbulent fluxes and concentration profiles. This numerical setup is meant to provide insight into the lowest $O(1\,\text{m})$ portion of the atmospheric surface layer, where water droplets or sand/dust grains will experience inertial influences on their trajectories between the time they are emitted and the subsequent transport throughout the whole PBL.

We find that while the primary balance governing the concentration of suspended particles remains between turbulent flux and gravitational settling, both fluxes are reduced in magnitude and cause a reduction of particle concentration at a specific height. This reduction in concentration increases with particle Stokes number, and reflects an inability of the particle to be instantaneously transported with the local fluid motion. Up to a Stokes number of approximately $St \approx 0.3$, the Equilibrium Eulerian framework provides a viable means for correcting the turbulent flux, and thus can reproduce inertial particle profiles accurately. Above this threshold, however, this first-order correction fails to reproduce behavior seen by the Lagrangian particles. In all cases, as the Stokes number is increased, the turbulent flux becomes less well represented by a similarity-based eddy diffusivity, and any attempt at parameterizing the vertical turbulent flux must begin with a more accurate description of the effective, inertia-influenced eddy diffusivity.

The result is that atmospheric weather prediction or large eddy simulation models, which attempt to predict the transport of spray, dust, snow, etc., may overestimate airborne concentrations if an inertialess, similarity-based theory is used to link traditional emission schemes (e.g., saltation models, sea spray generation functions) to the flux at the first grid point above the lower surface. Likewise in practice, surface emission parameterizations may underestimate true emission if airborne concentration observations are used to infer surface fluxes. Since particles must traverse through the first several meters of the surface layer before arriving at elevations corresponding to the first grid point in numerical models, they have necessarily experienced some inertial transport along the way. The present results suggest that this inertial behavior may result in a decrease in vertical fluxes compared to traditional predictions.

5 Acknowledgments

DR was supported by the National Science Foundation (NSF) under Grant No. AGS-1429921 and the Office of Naval Research (ONR) under Grant No. N00014-16-1-2472. MC was supported by NSF Grant No. AGS-1358593. The authors would like to thank the Computing Research Center at the University of Notre Dame for computational support. The authors would also like to acknowledge high-performance computing support from Yellowstone (UNDM0004), maintained by the Computational Information Systems Laboratory at the National Center for Atmospheric Research (NCAR). NCAR is supported by the NSF.

References

Aliseda A, Cartellier A, Hainaux F, Lasheras JC (2002) Effect of preferential concentration on the settling velocity of heavy particles in homogeneous isotropic turbulence. J Fluid Mech 468:77–105, DOI 10.1017/S0022112002001593

Anderson RS, Haff PK (1988) Simulation of eolian saltation. Science 241:820–823, DOI 10.1126/science.241.4867.820

Baas ACW (2008) Challenges in aeolian geomorphology: Investigating aeolian streamers. Geomorphology 93:3–16, DOI 10.1016/j.geomorph.2006.12.015

Balachandar S (2009) A scaling analysis for pointparticle approaches to turbulent multiphase flows. Int J Multiphase Flow 35(9):801–810, DOI 10.1016/j.ijmultiphaseflow.2009.02.013

Balachandar S, Eaton JK (2010) Turbulent dispersed multiphase flow. Annu Rev Fluid Mech 42:111–133, DOI 10.1146/annurev.fluid.010908.165243

Belan S, Lebedev V, Falkovich G (2016) Particle dispersion in the neutral atmospheric surface layer. Boundary-Layer Meteorol 159:23–40, DOI 10.1007/s10546-015-0108-7

Chamberlain AC (1967) Transport of Lycopodium spores and other small particles to rough surfaces. Proc Roy Soc 296(444):45–70, DOI 10.1098/rspa.1974.0120

Chamecki M, Meneveau C (2011) Particle boundary layer above and downstream of an area source: scaling, simulations, and pollen transport. J Fluid Mech 683:1–26, DOI 10.1017/jfm.2011.243

Chamecki M, Meneveau C, Parlange MB (2009) Large eddy simulation of pollen transport in the atmospheric boundary layer. J Aerosol Sci 40:241–255, DOI 10.1016/j.jaerosci.2008.11.004

Csanady GT (1963) Turbulent diffusion of heavy particles in the atmosphere. J Atmos Sci 20:201–208, DOI 10.1175/1520-0469(1963)020¡0201:TDOHPI¿2.0.CO;2

Druzhinin OA (1995) On the two-way interaction in two-dimensional particle-laden flows: the accumulation of particles and flow modification. J Fluid Mech 297:49–76, DOI 10.1017/S0022112095003004

Fairall CW, Larsen SE (1984) Dry deposition, surface production and dyamics of aerosols in the marine boundary layer. Atmos Env 18(1):69–77

Ferry J, Balachandar S (2001) A fast Eulerian method for disperse two-phase flow. Int J Multiphase Flow 27:1199–1226, DOI 10.1016/S0301-9322(00)00069-0

Fischer HB (1973) Longitudinal dispersion and turbulent mixing in open-channel flow. Annu Rev Fluid Mech 5:59–78, DOI 10.1146/annurev.fl.05.010173.000423

Freire LS, Chamecki M, Gillies JA (2016) Flux-profile relationship for dust concentration in the stratified atmospheric surface layer. Boundary-Layer Meteorol 160:249–267, DOI 10.1007/s10546-016-0140-2

Helgans B, Richter DH (2016) Turbulent latent and sensible heat flux in the presence of evaporative droplets. Int J Multiphase Flow 78:1–11, DOI 10.1016/j.ijmultiphaseflow.2015.09.010

Hoppel WA, Frick GM, Fitzgerald JW (2002) Surface source function for sea-salt aerosol and aerosol dry deposition to the ocean surface. J Geophys Res 107(D19):1–17, DOI 10.1029/2001JD002014

Kind RJ (1992) One-dimensional aeolian suspension above beds of loose particles - A new concentration-profile equation. Atmos Env 26(5):927–931, DOI 10.1016/0960-1686(92)90250-O

Kleefeld C, O'Dowd CD, O'Reilly S, Jennings SG, Aalto P, Becker E, Kunz G, de Leeuw G (2002) Relative contribution of submicron and supermicron particles to aerosol light scattering in the marine boundary layer. J Geophys Res 107(D19):8103, DOI 10.1029/2000JD000262

Knippertz P, Todd MC (2012) Mineral dust aerosols over the Sahara: Meteorological controls on emission and transport and implications for modeling. Rev of Geophys 50:RG1007, DOI 10.1029/2011RG000362

Kok JF (2011) A scaling theory for the size distribution of emitted dust aerosols suggests climate models underestimate the size of the global dust cycle. Proc of the National Academy of Sciences 108(3):1016–1021, DOI 10.1073/pnas.1014798108

Lewis ER, Schwartz SE (2004) Sea Salt Aerosol Production: Mechanisms, Methods, Measurements, and Models - a Critical Review. American Geophysical Union

Maxey MR (1987) The gravitational settling of aerosol particles in homogeneous turbulence and random flow fields. J Fluid Mech 174:441–465, DOI 10.1017/S0022112087000193

Monin AS, Yaglom AM (1971) Statistical Fluid Mechanics Volume 1. Dover Publications, Inc., Cambridge, MA

Nemes A, Dasari T, Hong J, Guala M, Coletti F (2017) Snowflakes in the atmospheric surface layer: observation of particleturbulence dynamics. J Fluid Mech 814:592–613, DOI 10.1017/jfm.2017.13

O'Dowd CD, de Leeuw G (2007) Marine aerosol production: a review of the current knowledge. Philos Trans R Soc 365:1753–1774, DOI 10.1098/rsta.2007.2043

Pan Y, Chamecki M, Isard SA (2013) Dispersion of heavy particles emitted from area sources in the unstable atmospheric boundary layer. Boundary-Layer Meteorol 146(2):235–256, DOI 10.1007/s10546-012-9753-2

Peters K, Eiden R (1992) Modelling the dry deposition velocity of aerosol particles to a spruce forest. Atmos Env 26(14):2555–2564, DOI 10.1016/0960-1686(92)90108-W

Pomeroy JW, Male DH (1992) Steady state suspension of snow. J Hydrol 136:275–301, DOI 10.1016/0022-1694(92)90015-N

Prandtl L (1952) Essentials of Fluid Dynamics with Applications to Hydraulics, Aeronautics, Meteorology, and Other Subjects. Hafner Publishing Company

Reeks MW (1983) The transport of discrete particles in inhomogeneous turbulence. J Aerosol Sci 14(6):729–739, DOI 10.1016/0021-8502(83)90055-1

Reid JS, Brooks B, Crahan KK, Hegg DA, Eck TF, O'Neill N, de Leeuw G, Reid EA, Anderson KD (2006) Reconciliation of coarse mode sea-salt aerosol particle size measurements and parameterizations at a subtropical ocean receptor site. J Geophys Res 111:D02,202, DOI 10.1029/2005JD006200

Richter DH, Sullivan PP (2013) Momentum transfer in a turbulent, particle-laden Couette flow. Phys Fluids 25:053,304, DOI 10.1063/1.4804391

Richter DH, Sullivan PP (2014) The sea spray contribution to sensible heat flux. J Atmos Sci 71(2):640–654, DOI 10.1175/JAS-D-13-0204.1

Righetti M, Romano GP (2004) Particle-fluid interactions in a plane near-wall turbulent flow. J Fluid Mech 505:93–121, DOI 10.1017/S0022112004008304

Rosenberg PD, Parker DJ, Ryder CL, Marsham JH, Garcia-Carreras L, Dorsey JR, Brooks IM, Dean AR, Crosier J, McQuaid JB, Washington R (2014) Quantifying particle size and turbulent scale dependence of dust flux in the Sahara using aircraft measurements. J Geophys Res Atmos 119:7577–7598, DOI 10.1002/2013JD021255

Rosenfeld D, Lohmann U, Raga GB, O'Dowd CD, Kulmala M, Fuzzi S, Reissell A, Andreae MO (2008) Flood or drought: how do aerosols affect precipitation? Science 321:1309–1313, DOI 10.1126/science.1160606

Rouse H (1937) Modern conceptions of the mechanics of fluid turbulence. American Society of Civil Engineers Transactions 102

Rouson DWI, Eaton JK (2001) On the preferential concentration of solid particles in turbulent channel flow. J Fluid Mech 428:149–169, DOI 10.1017/S0022112000002627

Sardina G, Schlatter P, Brandt L, Picano F, Casciola CM (2012) Wall accumulation and spatial localization in particle-laden wall flows. J Fluid Mech 699:50–78, DOI 10.1017/jfm.2012.65

Slinn SA, Slinn WGN (1980) Predictions for particle deposition on natural waters. Atmos Env 14:1013–1016, DOI 10.1016/0004-6981(80)90032-3

Slinn WGN (1982) Predictions for particle deposition to vegetative canopies. Atmos Env 16(7):1785–1794, DOI 10.1016/0004-6981(82)90271-2

Soldati A, Marchioli C (2009) Physics and modelling of turbulent particle deposition and entrainment: Review of a systematic study. Int J of Multiphase Flow 35:827–839, DOI 10.1016/j.ijmultiphaseflow.2009.02.016

Spalart PR, Moser RD, Rogers MM (1991) Spectral methods for the Navier-Stokes equations with one infinite and two periodic directions. J Computl Phys 96:297–324, DOI 10.1016/0021-9991(91)90238-G

Toba Y (1965) On the giant sea-salt particles in the atmosphere I. General features of the distribution. Tellus 17(1):131–145, DOI 10.1111/j.2153-3490.1965.tb00202.x

Vreman AW (2015) Turbulence attenuation in particle-laden flow in smooth and rough channels. J Fluid Mech 773:103–136, DOI 10.1017/jfm.2015.208

Wang LP, Maxey MR (1993) Settling velocity and concentration distribution of heavy particles in homogeneous isotropic turbulence. J Fluid Mech 256:27–68, DOI 10.1017/S0022112093002708

Wang LP, Stock DE (1993) Dispersion of heavy particles by turbulent motion. J Atmos Sci 50(13):1897–1913, DOI 10.1175/1520-0469(1993)050¡1897:DOHPBT¿2.0.CO;2

Zhang L, Gong S, Padro J, Barrie L (2001) A size-segregated particle dry deposition scheme for an atmospheric aerosol module. Atmos Env 35(3):549–560, DOI 10.1016/S1352-2310(00)00326-5